A DIFFUSION SYNTHETIC ACCELERATION SCHEME FOR RECTANGULAR GEOMETRIES BASED ON BILINEAR DISCONTINUOUS FINITE ELEMENTS

Bruno Turcksin and Jean C. Ragusa*
Department of Nuclear Engineering
Texas A&M University
bruno.turcksin@neo.tamu.edu; jean.ragusa@tamu.edu

ABSTRACT

A DSA technique to accelerate the iterative convergence of S_n transport solves is derived for bilinear discontinuous (BLD) finite elements on rectangular grids. The diffusion synthetic acceleration equations are discretized using BLD elements by adapting the Modified Interior Penalty technique, introduced in [4] for triangular grids. The MIP-DSA equations are SPD and thus are solved using a preconditioned CG technique. Fourier analyses and implementation of the technique in a BLD S_n transport code show that the technique is stable is effective.

Key Words: diffusion synthetic acceleration (DSA), bilinear discontinuous finite element (BLD)

1. INTRODUCTION

The Discontinuous Finite Element Method (DFEM) is a common spatial discretization technique for the discrete-ordinate (S_n) transport equations. The scattering source is usually converged using either a Richardson method, i.e., the Source Iteration (SI) technique, or a Krylov subspace approach (typically GMRes). For highly diffusive materials in optically thick configurations, these iterative techniques can become quite ineffective, requiring high iteration counts. However, SI and GMRes-based transport solves can be accelerated (preconditioned) with DSA approaches [1], leading to preconditioned Richardson and preconditioned GMRes versions, respectively. Yet, it is also well established that the spatial discretization of the DSA equations must be "consistent" with the one used for the S_n transport equations to yield unconditionally stable and efficient DSA schemes ([1,3,6,5,4]). However, the search for full consistency between the discretized transport equations and the discretized diffusion may not be computationally practical [6] and some partially consistent DSA schemes have been analyzed for DFE discretizations of the transport (e.g., [5,4]).

Here, we present a bilinear discontinuous (BLD) finite element technique for the DSA equations. That is, the same spatial discretization is employed for both the S_n transport equation and the diffusion synthetic accelerator. There are several advantages for using the same finite element space in both discretizations: (a) many of the elementary matrices employed to discretize the transport operator are also used for the discretization of the DSA operator; (b) should a continuous finite element discretization (as in the case of the WLA method [5], for instance), be chosen to discretize the DSA equations on spatially adapted meshes, hanging nodes treatment is required in order to preserve the continuous nature of finite element solution; however, a discontinuous discretization would deal seamlessly with spatially adapted meshes. Our BLD discretization of the DSA equations is an extension of the MIP method, introduced in [4] for triangular meshes.

*Corresponding author

The remainder of the paper is as follows. In Section 2, we recall some of the traditional discontinuous finite element approximations utilized to solve the diffusion equation and present the symmetric interior penalty scheme. The SI and GMRes solution techniques for the S_n transport equations are briefly given in Section 3. In Section 4, the DSA equations for the Modified Interior Penalty (MIP) are given in the case of a bilinear discontinuous discretization. Fourier analyses and numerical results are presented in Section 5. We conclude and propose extensions to this work in Section 6.

2. DISCONTINUOUS FINITE ELEMENT DISCRETIZATIONS FOR THE DIFFUSION EQUATION

Discontinuous finite element approximations are well-established for elliptic equations; see, for instance, [2]. The interior penalty family of methods has its origin in Nitsche's weak enforcement of Dirichlet boundary conditions [7]: rather than imposing that the numerical solution be equal to the user-specified boundary value, Nitsche proposed to add the following term (appropriately weighted) in the weak formulation $\int_{\partial V}(\Phi^{Dir}-\Phi)^2$; here, Φ^{Dir} denotes the Dirichlet boundary value, Φ is the numerical solution, $\partial\mathcal{D}$ is the boundary of the computational domain $\mathcal{D}$. Later, the idea was extended to include any "interior interface" (i.e., interfaces between cells). Many variants of interior penalty methods have been derived over the years (see the review articles [2,8]). Below, we briefly recall the symmetric interior penalty technique applied to diffusion equation. In Section 4, this technique will be slightly modified for use as a Diffusion Synthetic Accelerator (DSA). Consider the following diffusion problem :

$$-\boldsymbol{\nabla}\cdot D\boldsymbol{\nabla}\phi+\Sigma_a\phi=Q_0 \text{ for } (x,y)\in\mathcal{D}=[0,L_x]\times[0,L_y], \tag{1}$$

$$\frac{1}{4}\phi-\frac{1}{2}D\partial_n\phi=J^{inc} \text{ for } (x,y)\in\partial\mathcal{D}. \tag{2}$$

where D is the diffusion coefficient, ϕ is the scalar flux, Σ_a is the absorption cross section, Q_0 is a volumetric source, J^{inc} is an incoming current value; later, when employed as a DSA scheme, Q_0 will be changed to a fixed scattering source due to the difference in scalar fluxes after a transport sweep, i.e., $\Sigma_s(\Phi^{(\ell+1/2)}-\Phi^{(\ell)})$, and J^{inc} will be set to 0 since known angular fluxes at the boundary result in no error for the DSA equations, hence an incoming current equal to 0 (for brevity, we assume no reflective or periodic boundary conditions). The weak form for the symmetric interior penalty is given by (see, e.g., [2]):

$$b_{IP}(\phi,\varphi)=l_{IP}(\varphi), \tag{3}$$

where the bilinear form is:

$$\begin{aligned} b_{IP}(\phi,\varphi)=&(D\boldsymbol{\nabla}\phi,\boldsymbol{\nabla}\varphi)_{\mathcal{T}_h}+(\Sigma_a\phi,\varphi)_{\mathcal{T}_h}+(\kappa_e^{IP}[\![\phi]\!],[\![\varphi]\!])_{E_h^i}\\ &+([\![\phi]\!],\{\!\{D\partial_n\varphi\}\!\})_{E_h^i}+([\![\varphi]\!],\{\!\{D\partial_n\phi\}\!\})_{E_h^i}\\ &+\left(\kappa_e^{IP}\phi,\varphi\right)_{\partial\mathcal{D}}-\frac{1}{2}\left(\phi,D\partial_n\varphi\right)_{\partial\mathcal{D}}-\frac{1}{2}\left(D\partial_n\phi,\varphi\right)_{\partial\mathcal{D}} \end{aligned} \tag{4}$$

and the linear form is:

$$l_{IP}(\varphi)=(Q_0,\varphi)_{\mathcal{T}_h}+(J^{inc},\varphi)_{\partial\mathcal{D}}, \tag{5}$$

where $\mathcal{T}_h$ is the mesh used to discretize $\mathcal{D}$ into non-overlapping elements K, such that the union of the elements fully covers $\mathcal{D}$, E_h^i is the set of interior edges such that $E_h^i=\cup_{K_1,K_2\in\mathcal{T}_h}(\partial K_1\cap\partial K_2)$, and φ a bilinear discontinuous basis function. These BLD functions, given for the cell spanning $[0,\Delta x]\times[0,\Delta y]$,

are:

$$\varphi_1 = \frac{\Delta x - x}{\Delta x}\frac{\Delta y - y}{\Delta y}$$
$$\varphi_2 = \frac{x}{\Delta x}\frac{\Delta y - y}{\Delta y}$$
$$\varphi_3 = \frac{x}{\Delta x}\frac{y}{\Delta y}$$
$$\varphi_4 = \frac{\Delta x - x}{\Delta x}\frac{y}{\Delta y}$$

We also have defined the jump and mean values as:

$$[\![\phi]\!] = \phi^+ - \phi^-, \quad \{\!\{\phi\}\!\} = \frac{\phi^+ + \phi^-}{2}. \tag{6}$$

The penalty parameter κ_e^{IP} is given:

$$\kappa_e^{IP} = \begin{cases} \dfrac{C}{h_\perp}\dfrac{D^+ + D^-}{2} & \text{on interior edges, i.e., } e \in E_h^i, \\ C\dfrac{D}{h_\perp} & \text{on boundary edges, i.e., } e \in \partial\mathcal{D}, \end{cases} \tag{7}$$

where C is a constant (we used $C = 4$) and $h_\perp$ is the length of the cell in the direction orthogonal to edge e. The $+$ and $-$ symbols denote the values on either side of an edge. The notations implying summation over all elements and all interior edges are explained below:

$$(a,b)_{\mathcal{T}_h} = \sum_{K\in\mathcal{T}_h}\int_K a\,b\,dxdy$$
$$(a,b)_{E_h^i} = \sum_{e\in E_h^i}\int_e a\,b\,ds$$

with e denoting an edge and ds denoting an infinitesimal length along that edge.
It is important to note that the IP bilinear form, given in Eq. (4), is Symmetric Positive Definite (SPD); as such, very efficient techniques, such as preconditioned Conjugate Gradient (pCG) and Algebraic Multigrid (AMG) can be used to solve the associated linear system. In addition, the weak form is also relatively straightforward to implement, especially in xy rectangular geometries. Let the domain $\mathcal{D}$ be decomposed into a $n_x \times n_y$ cells and denote any cell in the domain by a pair of indices (i, j), where $1 \le i \le n_x$ and $1 \le j \le n_y$. Further assign the local vertex numbering $local = [1, 2, 3, 4]$ to the bottom-left, bottom-right, top-right, top-left vertices of any rectangular cell. Then, the global index of the bilinear unknowns in any cell (i, j) can be assigned as follows (this is just one possibility among others):

$$4\,(n_x(j-1) + (i-1)) + local(k) \qquad \text{for} \quad k = 1, ..., 4 \tag{8}$$

Thus, assembling the global diffusion may consist in two loops. One loop over the elements K in order to evaluate the volumetric terms in Eq. (4) and Eq. (5), and one loop over the set of edges (interior edges and boundary edges) in order to evaluate the edge terms in Eq. (4) and Eq. (5). All elementary matrices (for volumetric and surfacic terms appearing the weak form) are given in the Appendix for completeness.
In Fig. 1, we give a sample diffusion result obtained for the symmetric interior penalty formulation using BLD finite elements. The domain is 150×150, with homogeneous properties ($D = \frac{1}{3}$, $\Sigma_a = 0.1$), the external volumetric source is $Q_0 = 10$, vacuum boundaries are applied. The left pane in Fig. 1 shows the answer with a 10×10 grid, the right pane, with a 100×100 grid.

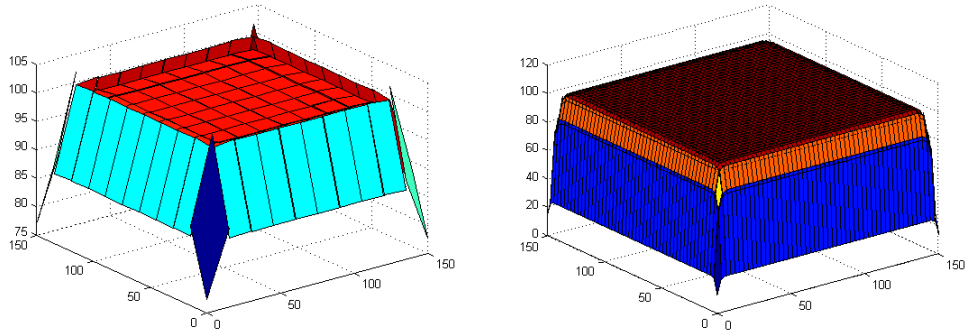

Figure 1: Solution of a diffusion equation based on the interior penalty method.

3. TRANSPORT SOLVES

The S_n transport equations (with isotropic source and scattering) are given by:

$$(\mathbf{\Omega}_d \cdot \boldsymbol{\nabla} + \Sigma_t(\mathbf{r}))\,\psi_d(\mathbf{r}) = \frac{1}{4\pi}\Sigma_s(\mathbf{r})\phi(\mathbf{r}) + \frac{1}{4\pi}S(\mathbf{r}), \quad \text{for } \mathbf{r} \in \mathcal{D},\ 1 \leq d \leq M \tag{9}$$

with $\psi_d(\mathbf{r}) = \psi(\mathbf{r}, \mathbf{\Omega}_d)$ the angular flux at position $\mathbf{r}$ in direction $\mathbf{\Omega}_d$, Σ_t and Σ_s the total and scattering cross sections, respectively. The scalar flux is defined as and evaluated as follows:

$$\phi(\mathbf{r}) \equiv \int_{4\pi} \psi(\mathbf{r}, \mathbf{\Omega}) d\mathbf{\Omega} \approx \sum_{d=1}^{M} w_d \psi_d(\mathbf{r}). \tag{10}$$

For brevity, we assume only incoming boundary conditions, $\psi_d(\mathbf{r}_b) = \psi_d^{inc}(\mathbf{r}_b)$, for any boundary location $\mathbf{r}_b \in \partial\mathcal{D}_d^- = \{\partial\mathcal{D} \text{ such that } \mathbf{\Omega}_d \cdot \boldsymbol{n}_b < 0\}$, where $\boldsymbol{n}_b = \boldsymbol{n}(\mathbf{r}_b)$ is the outward unit normal vector at the boundary. Eq. (9) can be written in a compact form using operators:

$$\boldsymbol{L}\Psi = \boldsymbol{M}\boldsymbol{\Sigma}\Phi + S \equiv q, \tag{11}$$

$$\Phi = \boldsymbol{D}\Psi. \tag{12}$$

Eq. (11)–Eq. (12) can be solved using the Source Iteration (SI) method (a stationary iterative technique also known as Richardson iteration). The SI technique at the ℓ^{th} iteration is given by :

$$\Phi^{(\ell+1)} = \boldsymbol{D}\boldsymbol{L}^{-1}\left(\boldsymbol{M}\boldsymbol{\Sigma}\Phi^{(\ell)} + S\right). \tag{13}$$

Alternatively, a subspace Krylov method (usually GMRes) can be employed to solve the system of equations:

$$\left(\boldsymbol{I} - \boldsymbol{D}\boldsymbol{L}^{-1}\boldsymbol{M}\boldsymbol{\Sigma}\right)\Phi = \boldsymbol{D}\boldsymbol{L}^{-1}S. \tag{14}$$

Both the SI and the GMRes approaches require transport sweeps (the action of $\boldsymbol{L}^{-1}$ is required in both procedures).

When the scattering ratio $c = \frac{\Sigma_s}{\Sigma_t}$ tends to one in optically thick domains, the number of SI and GMRes iterations can become large. To accelerate the convergence, a DSA preconditioner is needed; the Modified IP discontinuous finite element discretization of the diffusion equation for rectangular grids is presented next.

4. A BILINEAR DISCONTINUOUS DIFFUSION SYNTHETIC ACCELERATOR

The idea behind synthetic acceleration is that the error between the (yet unknown) transport solution and the latest SI iterate can be estimated from a computationally less expensive process, yielding a correction term to be added to the latest iterate in order to improve the next iterate. In DSA, the corrective scalar flux contribution is sought through the following diffusion solve, where the volumetric source term is due to the difference between successive iterates (and there are no surfacic source terms since the incoming angular flux was fully determined in the transport equation, thus the error diffusion problem is should be written with a vacuum boundary condition):

$$\boldsymbol{A}\,\delta\Phi = \boldsymbol{\Sigma}\left(\Phi^{(\ell+1/2)} - \Phi^{(\ell)}\right). \tag{15}$$

In our case, the diffusion matrix $\boldsymbol{A}$ is exactly the one obtained from the bilinear form Eq. (4), except for its penalty coefficient κ_e^{IP} being changed to κ_e^{MIP}, given below:

$$\kappa_e^{MIP} = \max\left(\frac{1}{4}\,,\,\kappa_e^{IP}\right). \tag{16}$$

In doing so, we followed [4] where the same modification of the penalty coefficient was performed for triangular meshes and Fourier analyses revealed the stability of the scheme. Our Fourier analyses for BLD are given in the Results Section below.

Then, the next SI iterate is obtained as follows:

$$\Phi^{(\ell+1)} = \Phi^{(\ell+1/2)} + \delta\Phi. \tag{17}$$

Similarly, DSA can be obtained to precondition GMRes transport solves. The final form of that system is:

$$\left(\boldsymbol{I} + \boldsymbol{A}^{-1}\boldsymbol{\Sigma}\right)\left(\boldsymbol{I} - \boldsymbol{D}\boldsymbol{L}^{-1}\boldsymbol{M}\boldsymbol{\Sigma}\right)\Psi = \left(\boldsymbol{I} + \boldsymbol{A}^{-1}\boldsymbol{\Sigma}\right)\boldsymbol{D}\boldsymbol{L}^{-1}S. \tag{18}$$

Both approaches, SI+DSA or DSA-preconditioned GMRes, require a linear system solve involving the diffusion matrix $\boldsymbol{A}$. Ideally, such a matrix should be SPD (such that efficient techniques can be employed in its linear solve) and easy to form (even on arbitrary grids).

Again, it is important to note that the preconditioned-SI and preconditioned GMRes systems require the solution of a linear system involving the diffusion matrix $\boldsymbol{A}$. This matrix is SPD and, therefore, pCG or AMG techniques will be employed to solve such systems. In this paper, matrix $\boldsymbol{A}$ is built and stored in compressed sparse row (CSR) format.

5. RESULTS

In this Section, we first present some Fourier analysis results for the SI+DSA solution techniques based on BLD discretizations of the transport and diffusion operators. Then, results from the implementation of MIP as a DSA preconditioner in a BLD transport code are provided.

5.1. Fourier Analyses for MIP-DSA using a BLD discretization

To analyze the performance of acceleration schemes, it is customary to carry out a Fourier Analysis (FA) on the discretized equations. A large body of work exists in the transport community regarding the application of FA to the study of acceleration of the SI scheme with DSA, both for the continuous and discretized equations [6]. Obviously, for numerical applications, the study of the discretized $\{\text{transport} + \text{acceleration}\}$ solvers is of prime interest. Here, we employ a periodic homogeneous domain. In FA analysis, the error is decomposed into modes that are charactered by Fourier wave numbers. How these modes are damped during one step of the SI+DSA scheme provides insight on the effectiveness of the acceleration method. This damping is characterized by the spectral radius, the largest attenuation factor for any wave number. The slowest mode will dominate as the iteration proceeds and its damping rate, i.e., the largest attenuation factor for any wave number or spectral radius, will eventually characterize the iteration procedure.

Fig. 2 presents the FA. The spectral radius is plotted as a function of the mesh optical thickness and the analysis are carried out for S_2 through S_{16}. The spectral radius is always less than 0.65 (worst situation is for S_2, for S_8 and higher order S_n quadratures, the spectral radius is less than ~ 0.4). In the fine mesh limit, the standard results from the 2D continuous Fourier analysis (that is, continuous in the sense of "not spatially discretized") are recovered: the spectral radius for S_2 is $0.5c$ and, as n increases, the spectral radius tends towards $0.2247c$. The results of Fig. 2 are very similar to the ones obtained in [4] on 2D triangular meshes.

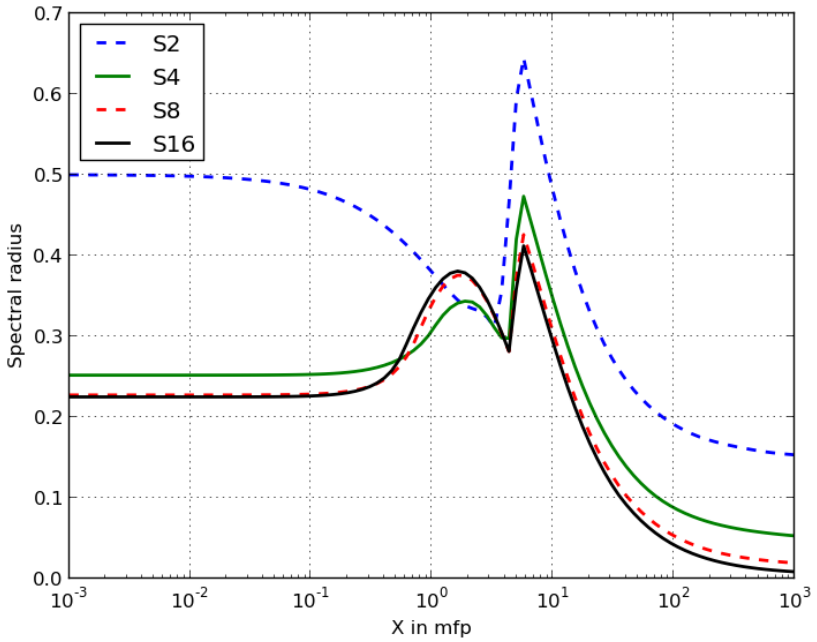

Figure 2: Fourier analysis for the MIP-DSA form as a function of the mesh optical thickness, homogeneous infinite medium case.

5.2. Numerical Results

The MIP-DSA technique has been implemented in an S_n transport code using rectangular cells and BLD DFE basis functions. The following test cases were run: the domain is square $100cm \times 100cm$ with vacuum boundaries. There are 10000 cells and we use BLD finite elements; there are 40000 degrees of freedom. The relative tolerance on SI is 10^{-8} and the relative tolerance on CG is 10^{-10}. We use a S_8 angular quadrature, $\Sigma_t = 1cm^{-1}$, and $\Sigma_s = 0.999cm^{-1}$. The source is uniform, $1n/(cm^3s)$. In the first test, the domain is discretized using 100 cells along x and 100 cells along y. In the second test, the domain is discretized using 250 cells along x and 40 cells along y; therefore, the aspect ratio is 6.25 for the second test. In the third test, the domain is discretized using 1000 cells along x and 10 cells along y (the aspect ratio is 100).

In Table I–Table III, we compare the CPU time and number of iterations for SI alone (no DSA), SI+DSA where the diffusion solves are carried out using unpreconditioned CG, and SI+DSA where the diffusion solves are carried out using CG preconditioned with AMG. In this Table, SI iter is the number of Source Iteration iterations needed to solve the problem, Prec is the time in seconds needed to initialize the preconditioner used by CG, MIP is the total time in seconds spent solving DSA during the calculation, CG iter is the total number of CG iterations used to solve MIP, and Total is the time in seconds needed to solve the problem. We note that solving the MIP equations requires more CG iterations when the aspect ratio increases, but when preconditioned with AMG, CG remains very efficient.

Table I: Comparison of preconditioners on rectangular mesh with an aspect ratio of 1.0 with BLD finite elements

	No-DSA	CG	AMG+CG
SI iter	7311	21	21
Prec (s)	NA	NA	0.057
MIP (s)	NA	39.4564	2.76611
CG iter	NA	8584	265
Total (s)	8254.46	66.8963	31.6606

Table II: Comparison of preconditioners on rectangular mesh with an aspect ratio of 6.25 with BLD finite elements

	No-DSA	CG	AMG+CG
SI iter	7311	23	23
Prec (s)	NA	NA	0.671
MIP (s)	NA	87.8195	4.20011
CG iter	NA	18985	171
Total (s)	7311.49	117.768	32.857

Table III: Comparison of preconditioners on rectangular mesh with an aspect ratio of 100 with BLD finite elements

	No-DSA	CG	AMG+CG
SI iter	7304	24	24
Prec (s)	NA	NA	0.383
MIP (s)	NA	361.306	3.74259
CG iter	NA	82613	177
Total (s)	8581.25	400.116	43.6815

6. CONCLUSIONS AND OUTLOOK

A discontinuous finite element technique based on the interior penalty method was used to solve the DSA equations in xy rectangular cells using BLD basis functions. Fourier analysis results show that the technique is stable and efficient, with a spectral radius of ~ 0.4 for S_8 and higher angular S_n quadratures. The discretized diffusion equations are SPD and thus are amenable to preconditioned CG linear solvers. Here, we also employed an algebraic multigrid technique. AMG was found to be very efficient, even for problems with cells presenting aspect ratios as high as 100.

In the future, we plan to extend this MIP-DSA technique to the PieceWise Linear Discontinuous (PWLD) technique for arbitrary polygons.

7. APPENDIX

For completeness, the elementary matrices needed to assemble the global diffusion matrix corresponding to the bilinear form Eq. (4) are given below. The BLD basis functions $(\varphi_k)_{1\leq k\leq 4}$ were given earlier, in Section 2.

Matrices' names that are **underlined and bold** are elementary matrices not present in the DFEM discretization of the transport equation. All other elementary matrices are already present in the transport discretization.

The **mass matrix** is given by :

$$M = \frac{\Delta_x \Delta_y}{36} \begin{pmatrix} 4 & 2 & 1 & 2 \\ 2 & 4 & 2 & 1 \\ 1 & 2 & 4 & 2 \\ 2 & 1 & 2 & 4 \end{pmatrix} \tag{19}$$

The **stiffness matrix** is given by :

$$S = \frac{\Delta_y}{6\Delta_x} \begin{pmatrix} 2 & -2 & -1 & 1 \\ -2 & 2 & 1 & -1 \\ -1 & 1 & 2 & -2 \\ 1 & -1 & -2 & 2 \end{pmatrix} + \frac{\Delta_x}{6\Delta_y} \begin{pmatrix} 2 & 1 & -1 & -2 \\ 1 & 2 & -2 & -1 \\ -1 & -2 & 2 & 1 \\ -2 & -1 & 1 & 2 \end{pmatrix} \tag{20}$$

The **horizontal edge mass matrix** (e.g., for angular flux upwinding on outgoing edge) is given by :

$$E_{M,h} = \frac{\Delta_x}{6} \begin{pmatrix} 2 & 1 \\ 1 & 2 \end{pmatrix} \tag{21}$$

The **horizontal coupling edge mass matrix** (e.g., for angular flux upwinding on incoming edge) is given by :

$$E^c_{M,h} = \frac{\Delta_x}{6}\begin{pmatrix} 1 & 2 \\ 2 & 1 \end{pmatrix} \tag{22}$$

The **vertical edge mass matrix** is given by :

$$E_{M,v} = \frac{\Delta_y}{6}\begin{pmatrix} 2 & 1 \\ 1 & 2 \end{pmatrix} \tag{23}$$

The **vertical coupling edge mass matrix** is given by :

$$E^c_{M,v} = \frac{\Delta_y}{6}\begin{pmatrix} 2 & 1 \\ 1 & 2 \end{pmatrix} \tag{24}$$

The **gradient edge mass matrix** $(\varphi, \partial_{\boldsymbol{n}}\varphi)_{E^i_h} = (\partial_{\boldsymbol{n}}\varphi, \varphi)^T_{E^i_h}$:

- **left edge** (right, top and bottom edge gradient coupling matrices are obtained in a similar manner)

$$\begin{aligned}
\int_0^{\Delta_y} \partial_x\varphi^T \cdot \varphi \, dy &= \int_0^{\Delta_y} \begin{pmatrix} -\frac{1}{\Delta_x}\frac{\Delta_y - y}{\Delta_y} \\ \frac{1}{\Delta_x}\frac{\Delta_y - y}{\Delta_y} \\ \frac{1}{\Delta_x}\frac{y}{\Delta_y} \\ -\frac{1}{\Delta_x}\frac{y}{\Delta_y} \end{pmatrix} \cdot \begin{pmatrix} \frac{\Delta_y - y}{\Delta_y} & 0 & 0 & \frac{y}{\Delta_y} \end{pmatrix} dy \\
&= \int_0^{\Delta_y} \begin{pmatrix} -\frac{1}{\Delta_x}\left(\frac{\Delta_y - y}{\Delta_y}\right)^2 & 0 & 0 & -\frac{1}{\Delta_x}\frac{\Delta_y y - y^2}{{\Delta_y}^2} \\ \frac{1}{\Delta_x}\left(\frac{\Delta_y - y}{\Delta_y}\right)^2 & 0 & 0 & \frac{1}{\Delta_x}\frac{\Delta_y y - y^2}{{\Delta_y}^2} \\ \frac{1}{a}\frac{\Delta_y y - y^2}{{\Delta_y}^2} & 0 & 0 & \frac{1}{a}\left(\frac{y}{\Delta_y}\right)^2 \\ -\frac{1}{a}\frac{\Delta_y y - y^2}{{\Delta_y}^2} & 0 & 0 & -\frac{1}{a}\left(\frac{y}{\Delta_y}\right)^2 \end{pmatrix} dy \\
&= \begin{pmatrix} -\frac{\Delta_y}{3\Delta_x} & 0 & 0 & -\frac{\Delta_y}{6\Delta_x} \\ \frac{\Delta_y}{3\Delta_x} & 0 & 0 & \frac{\Delta_y}{6\Delta_x} \\ \frac{\Delta_y}{6\Delta_x} & 0 & 0 & \frac{\Delta_y}{3\Delta_x} \\ -\frac{\Delta_y}{6\Delta_x} & 0 & 0 & -\frac{\Delta_y}{3\Delta_x} \end{pmatrix} \\
&= \frac{\Delta_y}{6\Delta_x}\begin{pmatrix} -2 & 0 & 0 & -1 \\ 2 & 0 & 0 & 1 \\ 1 & 0 & 0 & 2 \\ -1 & 0 & 0 & -2 \end{pmatrix}
\end{aligned} \tag{25}$$

The **gradient coupling-edge mass matrix** $(\varphi^{\pm}, \partial_{\boldsymbol{n}}\varphi^{\pm})_{E^i_h}$ and $(\partial_{\boldsymbol{n}}\varphi^{\pm}, \varphi^{\pm})_{E^i_h}$:

- **vertical edge** (right, top and bottom edge gradient coupling matrices are obtained in a similar

manner)

$$\begin{aligned}\left(\varphi^{-},\partial_x\varphi^{+}\right)_{E_h^i} &= \int_0^{\Delta_y}\partial_x\varphi^{+,T}\cdot\varphi^{-}\,dy\\ &= \int_0^{\Delta_y}\begin{pmatrix}-\frac{1}{{\Delta_x}^{+}}\frac{\Delta_y-y}{\Delta_y}\\ \frac{1}{{\Delta_x}^{+}}\frac{\Delta_y-y}{\Delta_y}\\ \frac{1}{{\Delta_x}^{+}}\frac{y}{\Delta_y}\\ -\frac{1}{{\Delta_x}^{+}}\frac{y}{\Delta_y}\end{pmatrix}\cdot\begin{pmatrix}0 & \frac{\Delta_y-y}{\Delta_y} & \frac{y}{\Delta_y} & 0\end{pmatrix}\\ &= \frac{\Delta_y}{6{\Delta_x}^{+}}\begin{pmatrix}0 & -2 & -1 & 0\\ 0 & 2 & 1 & 0\\ 0 & 1 & 2 & 0\\ 0 & -1 & -2 & 0\end{pmatrix}\end{aligned} \tag{26}$$

$$\begin{aligned}\left(\varphi^{+},\partial_x\varphi^{-}\right)_{E_h^i} &= \int_0^{\Delta_y}\partial_x\varphi^{-,T}\cdot\varphi^{+}\,dy\\ &= \int_0^{\Delta_y}\begin{pmatrix}-\frac{1}{{\Delta_x}^{-}}\frac{\Delta_y-y}{\Delta_y}\\ \frac{1}{{\Delta_x}^{-}}\frac{\Delta_y-y}{\Delta_y}\\ \frac{1}{{\Delta_x}^{-}}\frac{y}{\Delta_y}\\ -\frac{1}{{\Delta_x}^{-}}\frac{y}{\Delta_y}\end{pmatrix}\cdot\begin{pmatrix}\frac{\Delta_y-y}{\Delta_y} & 0 & 0 & \frac{y}{\Delta_y}\end{pmatrix}dy\\ &= \frac{\Delta_y}{6{\Delta_x}^{-}}\begin{pmatrix}-2 & 0 & 0 & -1\\ 2 & 0 & 0 & 1\\ 1 & 0 & 0 & 2\\ -1 & 0 & 0 & -2\end{pmatrix}\end{aligned} \tag{27}$$

$$\begin{aligned}\left(\partial_x\varphi^{+},\varphi^{-}\right)_{E_h^i} &= \int_0^{\Delta_y}\varphi^{-,T}\cdot\partial_x\varphi^{+}dy\\ &= \int_0^{\Delta_y}\begin{pmatrix}0\\ \frac{\Delta_y-y}{\Delta_y}\\ \frac{y}{\Delta_y}\\ 0\end{pmatrix}\cdot\begin{pmatrix}-\frac{1}{{\Delta_x}^{+}}\frac{\Delta_y-y}{\Delta_y} & \frac{1}{{\Delta_x}^{+}}\frac{\Delta_y-y}{\Delta_y} & \frac{1}{{\Delta_x}^{+}}\frac{y}{\Delta_y} & -\frac{1}{{\Delta_x}^{+}}\frac{y}{\Delta_y}\end{pmatrix}dy\\ &= \frac{\Delta_y}{6{\Delta_x}^{+}}\begin{pmatrix}0 & 0 & 0 & 0\\ -2 & 2 & 1 & -1\\ -1 & 1 & 2 & -2\\ 0 & 0 & 0 & 0\end{pmatrix}\end{aligned} \tag{28}$$

$$\begin{aligned}\left(\partial_x\varphi^{-},\phi^{+}\right)_{E_h^i} &= \int_0^{\Delta_y}\varphi^{+,T}\cdot\partial_x\varphi^{-}dy\\ &= \int_0^{\Delta_y}\begin{pmatrix}\frac{\Delta_y-y}{\Delta_y}\\ 0\\ 0\\ \frac{y}{\Delta_y}\end{pmatrix}\cdot\begin{pmatrix}-\frac{1}{{\Delta_x}^{-}}\frac{\Delta_y-y}{\Delta_y} & \frac{1}{{\Delta_x}^{-}}\frac{\Delta_y-y}{\Delta_y} & \frac{1}{{\Delta_x}^{-}}\frac{y}{\Delta_y} & -\frac{1}{{\Delta_x}^{-}}\frac{y}{\Delta_y}\end{pmatrix}dy\\ &= \frac{\Delta_y}{6{\Delta_x}^{-}}\begin{pmatrix}-2 & 2 & 1 & -1\\ 0 & 0 & 0 & 0\\ 0 & 0 & 0 & 0\\ -1 & 1 & 2 & -2\end{pmatrix}\end{aligned} \tag{29}$$

REFERENCES

[1] Marvin L. Adams and Edward W. Larsen. Fast iterative methods for discrete-ordinates particle transport calculations. *Progress in Nuclear Energy*, 40:3–159, 2002.

[2] Guido Kanschat. *Discontinuous Galerkin Methods for Viscous Incompressible Flow*. Springer, first edition, 2007.

[3] E. W. Larsen. Diffusion-Synthetic Acceleration Methods for Discrete-Ordinates Problems. *Transport Theory and Statistical Physics*, 13:107–126, 1984.

[4] Y. Wang and J.C. Ragusa. Diffusion Synthetic Acceleration for High-Order Discontinuous Finite Element S_n Transport Schemes and Application to Locally Refined Unstructured Meshes. *Nuclear Science and Engineering*, 166:145–166, 2010.

[5] T. A. Wareing, E. W. Larsen, and M. L. Adams. Diffusion Accelerated Discontinuous Finite Element Schemes for the Sn Equations in Slab and X-Y Geometries. *Proc. Int. Topl. Mtg. Adavances in Mathematics, Computations, and Reactor Physics, Pittsburgh, Pennsylvania*, April 28 - May 2 1991.

[6] James S. Warsa, Todd A. Wareing, and Jim E. Morel. Fully Consistent Diffusion Synthetic Acceleration of Linear Discontinuous S_N Transport Discretizations on Unstructured Tetrahedral Meshes. *Nuclear Science and Engineering*, 141(3):236–251, July 2002.

[7] J. Nitsche. Über ein Variationsprinzip zur Lösung von Dirichlet-Problemen bei der Verwendung von Teilräumen, die keinen Randbedingungen unterworfen sind. *Abh. Math. Univ. Hamburg*, 36:9–15, 1971.

[8] Douglas N. Arnold, Franco Brezzi, Bernardo Cockburn, L. Donatella Marini Unified Analysis Of Discontinuous Galerkin Methods For Elliptic Problems *Siam J. Numer. Anal.* , Vol. 39, No. 5, Pp. 17491779, 2002